

A Tunable Bandpass-to-Bandstop Reconfigurable Filter With Independent Bandwidths and Tunable Response Shape

Eric J. Naglich, *Student Member, IEEE*, Juseop Lee, *Member, IEEE*, Dimitrios Peroulis, *Member, IEEE*, and William J. Chappell, *Member, IEEE*

Abstract—The theory of bandpass-to-bandstop reconfigurable filters is developed in this work, and example filters are demonstrated. Designs are developed that allow for reconfigurable response shape and independent bandwidths in the bandpass and bandstop modes of the filter. These capabilities could potentially be useful in dynamic, open spectrums, concurrent transmit-receive systems, and multimode antenna array applications. The demonstrated filters were fabricated using substrate integrated evanescent-mode cavity resonators. The resonators are tuned using deformation of a copper membrane induced by a piezoelectric actuator. In measurement, a 1.06% 3-dB bandwidth bandpass filter with 2.6-dB passband insertion loss was switched to a 0.82% 3-dB S_{11} bandwidth bandstop filter with 45 dB of isolation.

Index Terms—Adaptive filters, cavity resonator filters, elliptic filters, switched filters, tunable filters.

I. INTRODUCTION

AS MODERN microwave systems are progressed toward spectrally cognitive operation, more and more filter reconfigurability will be necessary to enable the full potential of these systems' performance [1]. There has been much recent interest in tunable filters for cognitive systems, especially tunable bandpass filters. Some of these filters demonstrate relatively high Q values and can tune over an octave [2], and some have reconfigurable shapes [3]. Recent progress has also been made in tunable bandstop filters [4]. These bandstop filters are important in spectrally dense environments where interference is a large concern.

In an open spectrum with multiple cognitive radios simultaneously operating in it, an increasingly dynamic filter shape may be needed by a new radio for it to effectively join the environment. If this open environment contained several low-power interfering signals as in Fig. 1(a), this radio could need a narrowband bandpass filter centered at its receive frequency band to maximize the signal-to-noise ratio (SNR). If the environment changes so that it includes a higher power interferer that is spectrally close to the receive band of the radio, as in Fig. 1(b), the

Manuscript received June 03, 2010; revised August 20, 2010; accepted August 30, 2010. Date of publication November 11, 2010; date of current version December 10, 2010. This work was supported by the Defense Advanced Research Projects Agency Analog Spectral Processors Grant under program manager Sanjay Raman.

The authors are with the IDEAS Microwave Laboratory, Department of Electrical and Computer Engineering, Purdue University, West Lafayette, IN 47907 USA (e-mail: enaglich@purdue.edu; chappell@purdue.edu).

Color versions of one or more of the figures in this paper are available online at <http://ieeexplore.ieee.org>.

Digital Object Identifier 10.1109/TMTT.2010.2086533

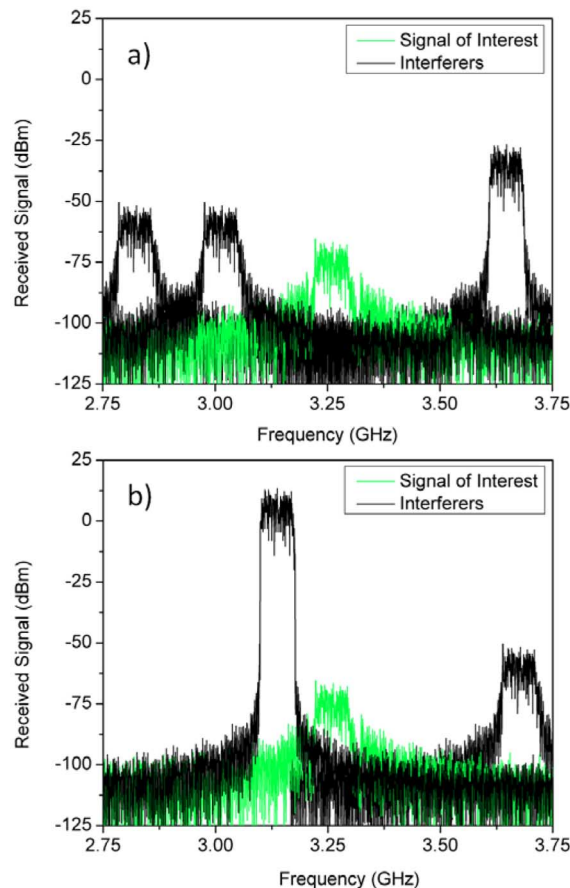


Fig. 1. (a) Spectrum where a bandpass filter would be most useful for isolating the signal of interest. (b) Spectrum where a bandstop filter would be most useful for isolating the signal of interest. These signals were adapted from an Agilent ADS example WCDMA project.

radio may lose its ability to resolve desired signals well. In this situation, the SNR could possibly be maximized if the radio was able to place a deep bandstop filter response at the high-power interferer's frequency of operation. In addition, if the new radio has a high-power transmitter, the existing radios may need to dynamically place a transmission null at the new radio's operating frequency so that they can maximize their levels of performance in the changed spectral environment.

Filters occupy a relatively large amount of physical space in modern wireless systems compared with other typical radio components, most of which are now easily integrated on chip. In many cases, it would be impractical to implement both tunable bandpass filter banks and tunable bandstop filter banks in

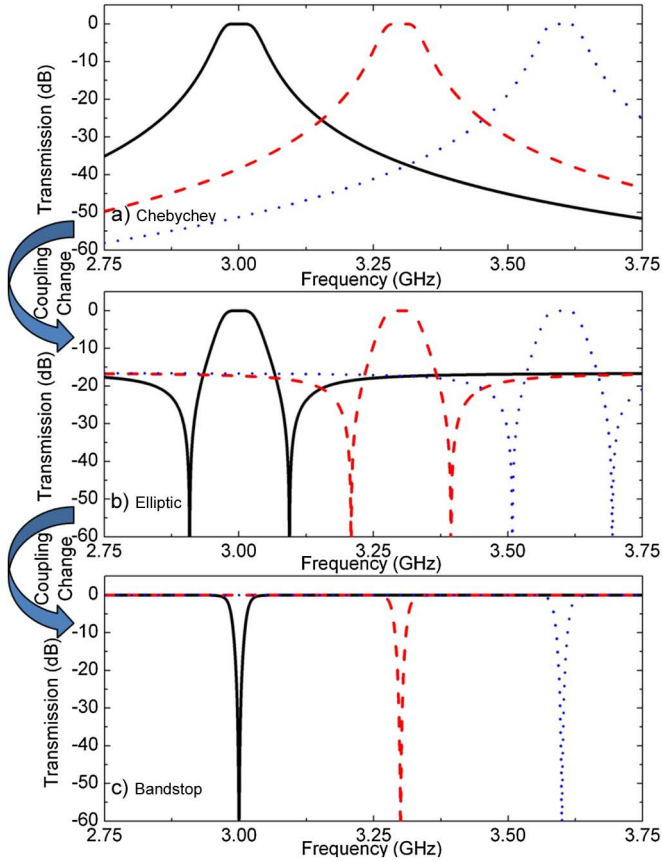


Fig. 2. Simulated results showing possible S_{21} responses of a set of two tunable resonators with tunable external and/or source-load coupling values.

a system due to size constraints. A possible solution to this problem is to implement sets of coupled resonators whose response can be dynamically switched between a bandpass and bandstop shape, saving space while providing added flexibility to a system. Fig. 2 shows that Chebyshev bandpass, elliptic bandpass, and bandstop responses can be obtained from the same set of resonators if their coupling values are tunable. Note that Fig. 2 is theoretical, and the ability to achieve all three responses in Fig. 2 would require components that have wider tuning ranges than what is commercially available today. However, with the wide array of switches and varactors that are available today, the theory presented below can be used to implement a filter that can transform between any single bandpass filter shape and any single bandstop filter shape. Fig. 3 shows the coupling diagram of the theoretical structure needed to implement the responses shown in Fig. 2. The dashed lines represent tunable or switchable coupling values, and the solid line represents static coupling.

A filter with the ability to switch between Chebyshev bandpass, elliptic bandpass, and “off” responses was shown in [5]. In contrast, the filter presented in this work switches between designed bandpass and bandstop filter responses, which is fundamentally different functionality. Bandpass-to-bandstop filter reconfigurability has been achieved in [6] and [7]. However, the filters demonstrated in these papers are not tunable and use relatively low Q resonators that result in spectrally wide responses. The filter in [6] uses the frequency-selective behavior

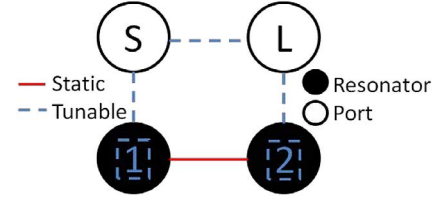


Fig. 3. Coupling diagram needed for implementation of a filter with responses shown in Fig. 2. Note that the resonant frequencies of the two resonators are independently tunable.

of a cascade of unit electromagnetic bandgap (EBG) structures that can be switched to exhibit either a bandpass or bandstop response, and [7] demonstrates a bandpass-to-bandstop filter with a closed-ring resonator whose reconfigurability results from the perturbation effect on degenerate modes. In contrast, this work demonstrates a filter that can switch between many commonly prescribed narrowband filter functions. For example, the theory described in this paper could be used to create a filter that could switch between a Butterworth bandpass response and a Chebyshev bandstop response. In general, while the previous solutions are innovative, bandpass-to-bandstop reconfigurable filters suitable for integration into a tunable, narrowband system have not been demonstrated. This work develops the theory of narrowband, prescribed-response, bandpass-to-bandstop electronically reconfigurable filters and demonstrates a novel, high- Q , tunable, evanescent-mode cavity design with new capabilities not found in previous designs.

II. BANDPASS-TO-BANDSTOP RECONFIGURABLE FILTER THEORY

The same geometry resonators can be used for a bandpass or a bandstop filter if the coupling relationships between the source, load, and resonators are changed appropriately. For the second-order filter analysis in this work, both external coupling values will be equal to each other, the resonator self-coupling values will have the same magnitude but opposite sign, and symmetries such as the source-to-load coupling being the same as the load-to-source coupling can be taken advantage of to simplify the generalized second-order filter $(N + 2) \times (N + 2)$ coupling matrix \mathbf{M} as shown in

$$\mathbf{M} = \begin{bmatrix} 0 & M_{01} & 0 & M_{03} \\ M_{01} & M_{11} & M_{12} & 0 \\ 0 & M_{12} & -M_{11} & M_{01} \\ M_{03} & 0 & M_{01} & 0 \end{bmatrix} \quad (1)$$

where the subscripts 0 and 3 correspond to the source and load, respectively, and subscripts 1 and 2 correspond to the first and second resonators, respectively.

It can be shown with coupling matrix methods [8] that the coupling matrix for a typical second-order Butterworth bandpass filter is

$$\mathbf{M} = \begin{bmatrix} 0 & 0.8409 & 0 & 0 \\ 0.8409 & 0 & 0.7071 & 0 \\ 0 & 0.7071 & 0 & 0.8409 \\ 0 & 0 & 0.8409 & 0 \end{bmatrix} \quad (2)$$

and the coupling matrix for a second-order Butterworth bandstop filter is

$$\mathbf{M} = \begin{bmatrix} 0 & 1.189 & 0 & 1 \\ 1.189 & 0 & 0 & 0 \\ 0 & 0 & 0 & 1.189 \\ 1 & 0 & 1.189 & 0 \end{bmatrix}. \quad (3)$$

Compared to the bandstop filter in (3), the coupling matrix in (2) has two main differences. Typical bandstop filters have a source to load coupling (M_{03}) value equal to one, which is commonly implemented as a 90° transmission line. Also, common bandstop filters have an interresonator coupling (M_{12}) value of zero, indicating that bandstop filters place the resonators in a shunt configuration, while bandpass filters, with a nonzero M_{12} and zero-valued M_{03} , place the resonators in a series configuration. In addition to these two differences, the M_{01} value changes slightly between the bandpass and bandstop cases. M_{01} becomes 1.189 in the normalized frequency Butterworth bandstop case, compared with 0.8409 for the Butterworth bandpass case.

It is straightforward to change the zero-valued M_{03} of a bandpass filter to a value of one through the use of switches with high isolation which switch in a 90° transmission line between the resonators. In addition, a uniquely designed coupling structure will be shown below that allows for the switching of M_{01} between the bandpass and bandstop modes of the filter. However, changing from a nonzero M_{12} value to an M_{12} value of zero is very difficult in practice, since it is difficult to fully block the coupling mechanism between resonators. Fortunately, it is possible to synthesize a bandpass-to-bandstop reconfigurable filter with a nonzero M_{12} value if the resonators of the filter can be tuned asynchronously [9].

The analysis in [9] begins with the general coupling matrix for a conventional bandstop filter with synchronously tuned resonators. An example can be seen in (3) for a synchronously tuned Butterworth bandstop filter. However, [9] shows that (3) is just one of many possible Butterworth bandstop filter coupling matrices. If (3) is allowed to have nonzero M_{11} and M_{12} values as in (1), an infinite number of Butterworth bandstop filter coupling matrices is possible. Reference [9] shows that, as long as

$$M_{01}^2 (M_{12} + M'_{12}) + M_{12}^2 > M_{12}'^2 \quad (4)$$

is satisfied, where primed quantities correspond to the new, asynchronously tuned filter and unprimed quantities correspond to the original, synchronously tuned filter, the same frequency response can be achieved with an arbitrary M'_{12} value if

$$M'_{11} = \pm \sqrt{M_{01}^2 (M_{12} + M'_{12}) + M_{12}^2 - M_{12}'^2} \quad (5)$$

is satisfied and $M'_{01} = M_{01}$. In this example, M_{12} , which is the inter-resonator coupling for the synchronously tuned bandstop filter in (3), is zero. For an M'_{12} of one, an M_{11} of 0.643 produces the Butterworth response of the original synchronously tuned filter.

In most cases, the desired bandpass and bandstop response \mathbf{M} matrices will have different M_{12} values. However, it is possible to implement both matrices without a tunable physical inter-resonator coupling structure in a filter. In a physical filter imple-

mentation at microwave frequencies, the inter-resonator coupling coefficient k_{12} can sometimes describe coupling values between resonators more clearly since it accounts for bandwidth explicitly. This is especially appropriate in a filter with two modes of operation, where each mode has different semi-arbitrary fractional bandwidths. In this case, k_{12} will be constant between filter modes of operation for a static physical inter-resonator coupling structure, but M_{12} will change due to differing fractional bandwidths in each mode of filter operation. In other words, using k_{12} instead of M_{12} will more clearly show that the inter-resonator coupling is static throughout the synthesis process. Because of this, the remainder of the theoretical analysis in this paper will be done using the coupling coefficients k_{01} and k_{12} along with M_{01} and M_{12} as follows:

$$\begin{aligned} k_{01} &= \sqrt{\Delta} \cdot M_{01} \\ k_{12} &= \Delta \cdot M_{12} \end{aligned} \quad (6)$$

where Δ is fractional bandwidth. It is to be understood that k_{01} represents external coupling to both of the filter's ports because both coupling values will always be equal in this analysis.

Using the k values in (6) to represent coupling values at the actual design fractional bandwidths will allow straightforward synthesis of a bandpass-to-bandstop reconfigurable filter with independent bandwidths for each mode of operation without a tunable k_{12} value. It will be shown that a bandpass-to-bandstop reconfigurable response can be synthesized by enabling tunable coupling values for k_{01} , M_{11} , and M_{03} only and that k_{12} can be static and arbitrary as long as (4) is satisfied. It is also possible to change M_{03} to produce an elliptic response in the bandpass case. First, the novel coupling structure used in the proposed filter will be explained.

A. Novel Coupling Structure for Simultaneous k_{01} and M_{03} Switching

The novel coupling structure designed for bandpass-to-bandstop reconfigurable filters is a transmission line of electrical length L degrees over a coupling aperture in the wall of the first resonator, followed by a switch, followed by a transmission line of length $270 - 2 \cdot L$ degrees, followed by a switch, followed by a transmission line of length L degrees over a coupling aperture in the wall of the second resonator. A model of such a structure can be seen in Fig. 4, where the resonators have been omitted for clarity.

This coupling structure has three modes of operation. First, in the bandstop mode of the filter, the switches are closed, and the coupling structure becomes a 270° transmission line over coupling apertures in the resonators. A 270° transmission line has a positive coupling value in this analysis. This positive insertion phase allows for a bandstop response with a nonzero k_{12} value. The coupling apertures in the walls of the resonators are sized to provide the appropriate k_{01} value for the bandstop mode of the filter. An equivalent circuit model of this mode of operation can be seen in Fig. 5(a).

The coupling structure's second mode of operation requires very high isolation switches. In this mode, the switches are open, and the coupling structure becomes a transmission line of length L degrees over a coupling aperture in the in the wall of the first

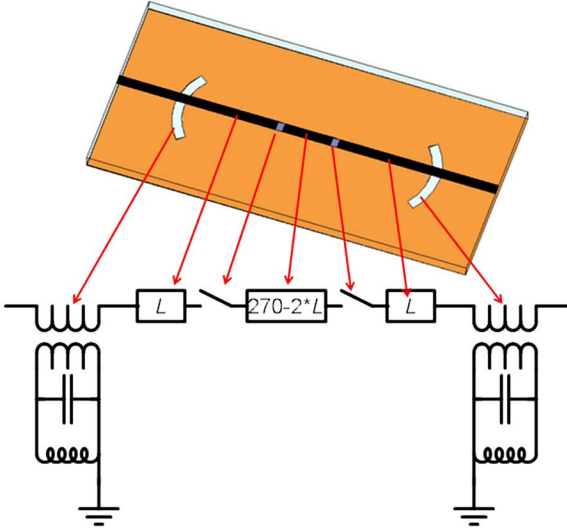


Fig. 4. Novel coupling structure designed for bandpass-to-bandstop reconfigurable filters.

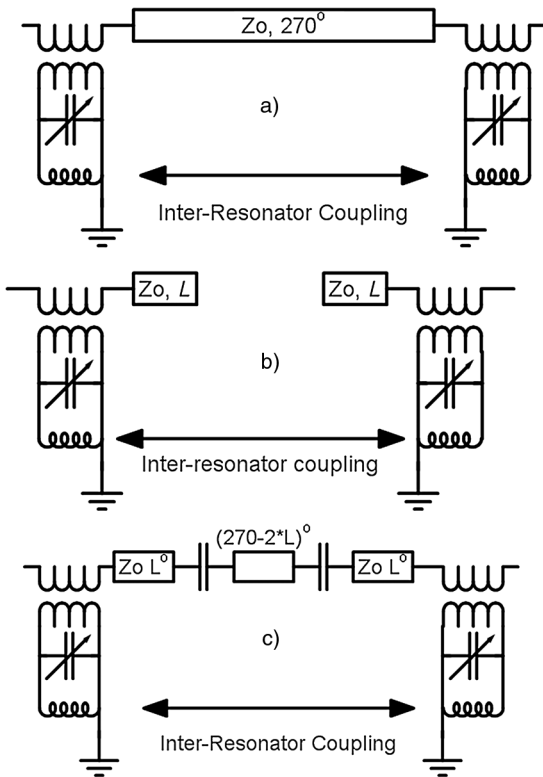


Fig. 5. (a) Coupling structure in the bandstop mode of the filter. (b) Coupling structure in the bandpass mode with very high isolation switches. (c) Coupling structure in the bandpass mode with medium isolation switches, enabling an elliptic response.

resonator. The transmission line between the two switches is not coupled to, therefore the source to load coupling is removed. Symmetry allows similar coupling into resonator 2 as resonator 1. The transmission lines of length L are approximately open at their interior ends if high-isolation switches are utilized. The length of the transmission line from the coupling aperture to the

open end transforms the impedance seen at the coupling aperture. Therefore, k_{01} also changes accordingly, and different k_{01} values are possible between the bandpass and bandstop modes of the filter. An equivalent circuit for this mode of operation can be seen in Fig. 5(b).

The coupling structure's third mode of operation requires a switch with a medium level of isolation, similar to the level found in common solid-state RF switches. Variable isolation switches or varactors could also be used for even more flexibility. In this mode, the switches are in their off-state but have significant capacitance. An equivalent circuit for this mode of operation can be seen in Fig. 5(c). For a certain range of small switch capacitance values, the capacitance shown in Fig. 5(c) adds approximately two more 90° phase shifts into the circuit. Considering that 270 electrical degrees are already present from the transmission lines, the total insertion phase in this mode of the coupling structure becomes 450° . This is a significant result because the 450° of insertion phase is the sign opposite of the 270° of insertion phase obtained in the bandstop mode of operation, and this allows for negative source-to-load coupling. Negative source-to-load coupling results in an elliptic response [10], [11], providing a third useful mode of operation for the proposed filter.

B. Analysis of Bandpass-to-Bandstop Reconfigurable Filter

In the typical bandpass mode of the filter, the second mode of operation of the coupling structure defined in Section II-A above is given by

$$\begin{aligned} k_{01BP} &= \sqrt{\Delta_{BP}} \cdot M_{01BP} \\ k_{12BP} &= \Delta_{BP} \cdot M_{12BP} \end{aligned} \quad (7)$$

where the subscript BP denotes quantities associated with the bandpass mode of the filter. As stated previously, it is desired to synthesize a bandpass-to-bandstop reconfigurable filter with a static k_{12} value. Therefore, in the bandstop mode of the filter,

$$\begin{aligned} k_{01BS} &= \sqrt{\Delta_{BS}} \cdot M_{01BS} \\ k_{12BS} &= k_{12BP} \end{aligned} \quad (8)$$

where the subscript BS denotes quantities associated with the bandstop mode of the filter. This corresponds to the first mode of operation of the coupling structure defined in Section II-A. Setting k_{12BP} equal to k_{12BS} is possible if the resonators of the filter are can be tuned asynchronously [9]. For an arbitrary k_{12BS} , the resonators must be tuned asynchronously according to the relationship in (9) and (10), which are modified versions of (5). These expressions must produce a real number value for M_{11} as follows:

$$M_{11BS} = \sqrt{M_{01BS}^2 M_{12BS} - M_{12BS}^2} \quad (9)$$

or

$$M_{11BS} = \sqrt{M_{01BS}^2 \left(\frac{k_{12BP}}{\Delta_{BS}} \right) - \left(\frac{k_{12BP}}{\Delta_{BS}} \right)^2}. \quad (10)$$

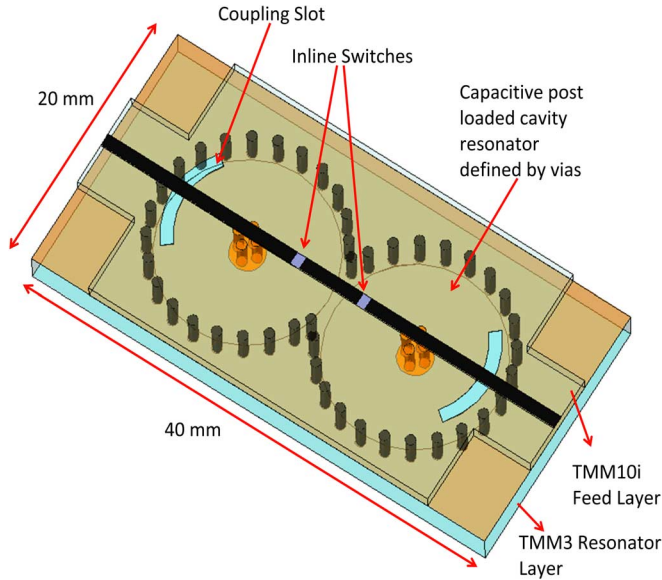


Fig. 6. Filter simulation model showing geometry and materials used in the fabricated filter.

The bandstop k and M values in (8)–(10) produce a bandstop filter which has a fractional bandwidth (FBW) lower limit of

$$\text{FBW}_{\text{BS min}} = \frac{k_{12\text{BP}}}{M_{01\text{BS}}^2} = \frac{\Delta_{\text{BP}} \cdot M_{12\text{BP}}}{M_{01\text{BS}}^2}. \quad (11)$$

Since $M_{12\text{BP}}/M_{01\text{BS}}^2 = 0.5$ using the values in (2) and (3), the bandstop filter must be at least half as wide in bandwidth as the bandpass filter for the case of switching a Butterworth bandpass filter to a Butterworth bandstop filter. However, other filter shapes can be used to produce different bandwidth limitations between each mode of operation.

III. BANDPASS-TO-BANDSTOP RECONFIGURABLE FILTER DESIGN

An evanescent-mode cavity-resonator-based bandpass-to-bandstop reconfigurable filter was fabricated with a static inter-resonator coupling structure for measurement. A model of the fabricated filter can be seen in Fig. 6. An expanded view of each layer of the structure is shown in Fig. 7. The evanescent-mode cavity resonators were designed in 3.175-mm-thick Rogers TMM3 printed circuit board material and defined by plated vias. The cavities have semi-circular apertures cut into their surface to enable magnetic field coupling. These resonators were loaded with capacitive posts to reduce their size for a given resonant frequency at the cost of quality factor (Q), but relatively high values of Q are still possible using this method [12]. Single, weakly coupled resonators were fabricated out of the same TMM3 board as the filter cavities presented in this paper, and the unloaded Q was measured to vary from 608 to 650 across the frequency range from 2.75 to 3.75 GHz.

A copper membrane was laminated onto the substrate to close the cavity and form the bottom plate of the capacitor inside of the resonator. Commercially available 0.38-mm-thick piezoelectric actuators from Piezo Systems were attached to the copper membrane to allow for electronically controllable deformation of the

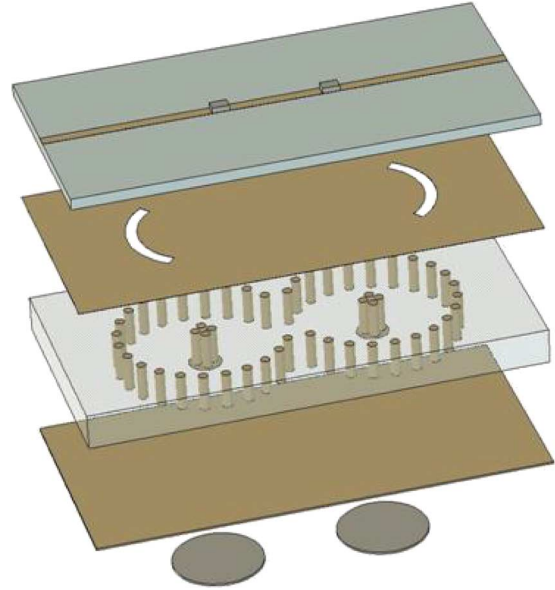


Fig. 7. Layer-by-layer expanded view of filter. From top to bottom, the layers are TMM10i, thin copper, TMM3, and thin copper. The disks represent the actuators. Note that there are switches in line with the transmission line shown above on the top layer.

membrane. This deformation changes the loading capacitance and thus the center frequency of the resonator. Capabilities of these resonators with associated bias voltages and capacitive gap dimensions can be seen in [12].

The cavity feeds were fabricated on 1.27-mm-thick Rogers TMM10i material and laminated to the cavities. The feeds were fabricated on this high-dielectric material to reduce the size of the 270° transmission line for source-to-load coupling described above.

The bandwidths of the bandpass and bandstop modes of the filter are somewhat independent. Each can be designed within the fractional bandwidth range of 0.5%–5.0%. The design of a second-order, independent-bandwidth, bandpass-to-bandstop reconfigurable filter like the one presented in this work can be completed by following the procedure outlined below. It is assumed at the start of this procedure that adequate resonators have already been designed and that magnetic coupling is used to physically implement M_{01} , such as the aperture coupling into the resonators shown in Fig. 7. Example values for a 1.2% fractional bandwidth Butterworth bandpass to 0.9% fractional bandwidth Butterworth bandstop reconfigurable filter will be given to aid understanding.

- Step 1) Design the coupling between the two resonators, k_{12} , as required by the bandpass shape that is desired [13]. This should be carried out as if only a bandpass filter was being designed. For example, in a second-order Butterworth bandpass filter as in (2), M_{12} is 0.7071. For a 1.2% fractional bandwidth, this results in a k_{12} of 0.008485.
- Step 2) Implement a source-to-load coupling value, M_{03} , of one with a phase of 270° degrees. A 270° transmission line whose characteristic impedance matches that of the system can be used to accomplish this.

- Step 3) Now, assuming a k_{12} value of zero, design the external coupling, k_{01} , as required to meet the bandwidth specification of the bandstop filter [14]. Use the M_{01} value from (3) for the normalized Butterworth bandstop filter, 1.189. For a 0.9% fractional bandwidth filter, this results in a k_{01} of 0.1128.
- Step 4) The k_{12} value is fixed by the bandpass mode of the filter at 0.008485. Since the bandstop filter has a 0.9% fractional bandwidth, an M_{12} value of 0.9428 describes the inter-resonator coupling in the bandstop mode.
- Step 5) To achieve the desired bandstop response, tune the resonators asynchronously according to (9) and (10). With the coupling values above, an M_{11} value of 0.6663 describes the resonator self-coupling for the bandstop mode of the filter.
- Step 6) Design the location of the switches along the 270° transmission line to enable switching between the k_{01} needed for the bandstop mode [step 3]) and the k_{01} needed for the bandpass mode [see (2) and (7)] [15]. When the switches are placed directly after the magnetic coupling structures for k_{01} , the minimum in external coupling is achieved for the case when the switch is open because the coupling structure is adjacent to a current minimum on the transmission line. When the switches are placed 90° in electrical length after the coupling structures for k_{01} , the maximum in external coupling is achieved for the case when the switch is open because the coupling structure is adjacent to a current maximum on the transmission line. The switches are closed in the bandstop mode, resulting in a 270° transmission line.
- Step 7) Determine the switch type and amount of switch isolation needed for the prescribed bandpass filter shape. A very high isolation switch with low off-state reactance will provide a Butterworth or Chebyshev response, as shown in Fig. 2(a). Isolation on the order of 40–50 dB is required for this example design. However, a lower isolation reflective switch with capacitive reactance in the off state will create an elliptic response, as shown in Fig. 2(b). The isolation level of the switches will be the limit of the out of band isolation in the elliptic bandpass case, unless the design has high source-to-load coupling through another mechanism. An absorptive switch will provide inductive reactance in its off state, and this will produce the response of a self-equalized filter. A theoretical progression of filter responses in the normalized frequency domain for changing switch isolation types and levels is shown in Fig. 8. Note that the location of the transmission zeros in the elliptic state of the filter can be designed through the choice of switch isolation, with the tradeoff being less filter isolation beyond the transmission zeros the closer the transmission zeros are to the filter passband.

In the 1.2% fractional bandwidth bandpass mode of the filter, the coupling matrix in (2) will describe the filter, and the k

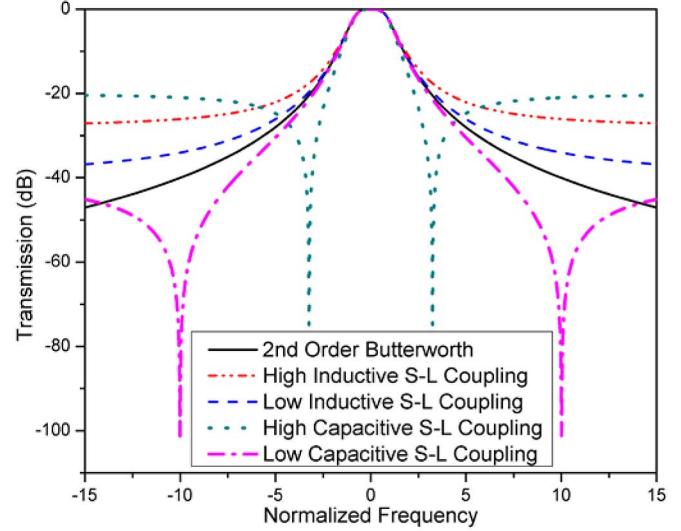


Fig. 8. Theoretical progression of filter responses in the normalized frequency domain for four different source-to-load coupling structure switch isolation levels. The second-order Butterworth response has zero source-to-load coupling.

values will be

$$\begin{aligned} k_{01BP} &= 0.09212 \\ k_{12BP} &= 0.008485. \end{aligned} \quad (12)$$

In the 0.9% fractional bandwidth bandstop mode of the filter, the coupling matrix in

$$\mathbf{M} = \begin{bmatrix} 0 & 1.189 & 0 & 1 \\ 1.189 & 0.6663 & 0.9428 & 0 \\ 0 & 0.9428 & -0.6663 & 1.189 \\ 1 & 0 & 1.189 & 0 \end{bmatrix} \quad (13)$$

will describe the filter.

The k values for the bandstop mode of the filter will be

$$\begin{aligned} k_{01BS} &= 0.11280 \\ k_{12BS} &= 0.008485. \end{aligned} \quad (14)$$

Notice that the k_{12} value in both modes of the filter is the same, enabling a static inter-resonator coupling structure. The difference in k_{01} between filter modes is designed for by the correct placement of the switches in the source to load coupling structure described above. Finally, the difference in M_{11} values can be implemented as long as the filter's resonators are independently tunable. Therefore, a tunable bandpass filter can be made a bandstop filter by simply putting a switch on the feed line structure, but only if the proper design rules are followed.

IV. MEASURED RESULTS

The response of the fabricated filter was measured using an Agilent Technologies N5230C PNA. Bias voltages were applied to the switches and piezoelectric actuators using Keithley 2400 Sourcemeter power supplies. Piezoelectric actuator bias voltages ranged from -200 to 0 V. A labeled photograph of the device can be seen in Fig. 9.

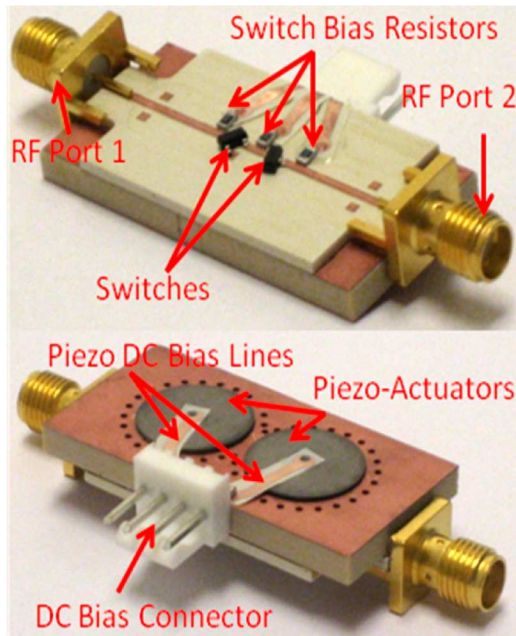


Fig. 9. Labeled photograph of both sides of the fabricated filter. For measurements, a network analyzer was connected to the RF ports, and dc power supplies were connected to the dc bias connector. The dc traces were fabricated on a $25.4\text{-}\mu\text{m}$ liquid crystal polymer (LCP) substrate.

The ideal synthesized response in Fig. 10(a) shows a theoretical second-order Butterworth bandpass filter with no stray coupling between source and load ports. It is valuable to do a measurement of the fabricated filter without switches in the source-to-load coupling structure to observe the amount of coupling due to radiation and substrate paths for comparison. This measurement can also be seen in Fig. 10(a). This response is the optimal limit of what could be achieved with this design. While this response is shown for reference, it may be possible to achieve a similar response with high-quality microelectromechanical systems (MEMS) switches [16] in the near future. The response of this filter in both bandstop and bandpass modes can be seen over a wider frequency range in Fig. 11. A zero-ohm resistor was used in the bandstop case in Fig. 11 to simulate a perfect switch and show the optimal limit of the design. The bandstop mode shows good performance up to 6 GHz, where an unwanted resonance starts to appear. The bandpass mode has 20 dB or greater out-of-band attenuation across the entire frequency range. Because of the extended upper stop band in the bandpass case, no spurious passband circuitry would be required in most systems.

A self-equalized filter response was produced by using state-of-the-art, absorptive, solid-state switches [17] with high isolation and low insertion loss. Synthesized and measured examples can be seen in Fig. 10(b). The measured plot in Fig. 10(c) was obtained using medium isolation reflective switches [18], resulting in an elliptic response. For the ideal case in Fig. 10(a), the filter is centered at 3.21 GHz and exhibits 2.6 dB of insertion loss in the passband. Of this loss, 0.12 dB is due to the fact that the filter has stronger external coupling than was designed for due to fabrication tolerances of the circuit board plotter used. Accounting for the mismatch loss, a 1%

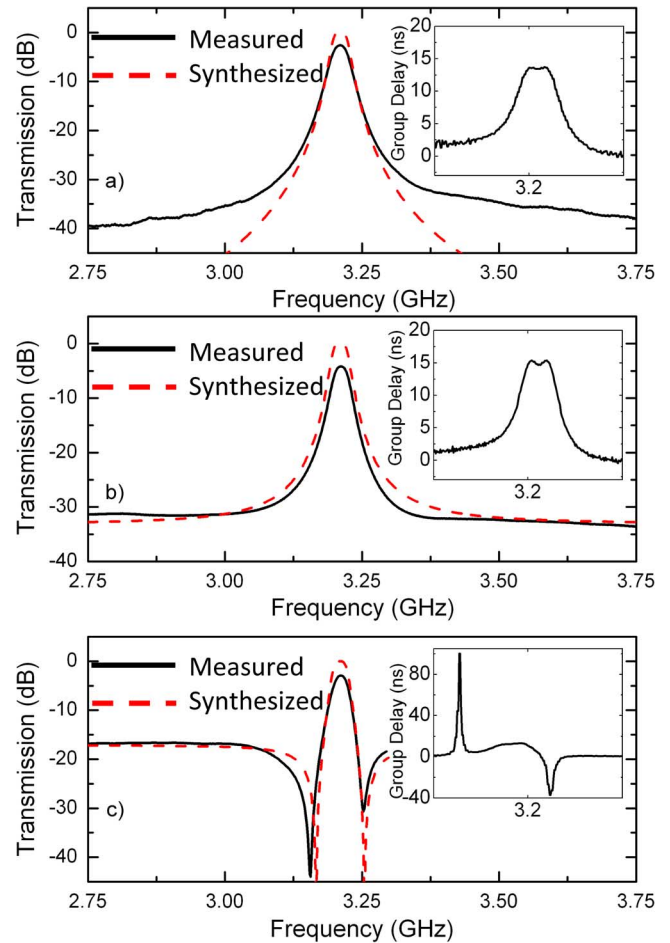


Fig. 10. Measured and synthesized S_{21} responses of the filter in the bandpass mode. (a) Response with no switches (open) compared with the ideal Butterworth filter. (b) Response with absorptive switches compared with the ideal self-equalized filter. (c) Response with reflective switches compared to ideal elliptic filter. Note that loss was not included in synthesis.

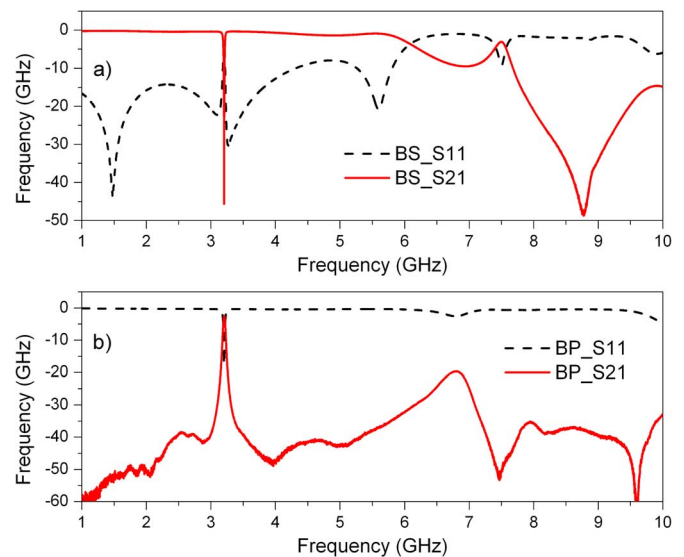


Fig. 11. Measured S_{11} and S_{21} responses of the filter in the bandpass and bandstop modes from 1 to 10 GHz. (a) Bandstop mode. (b) Bandpass mode.

fractional bandwidth filter with 2.5 dB of insertion loss has a Q of 457 based on gain-bandwidth product. Also, according

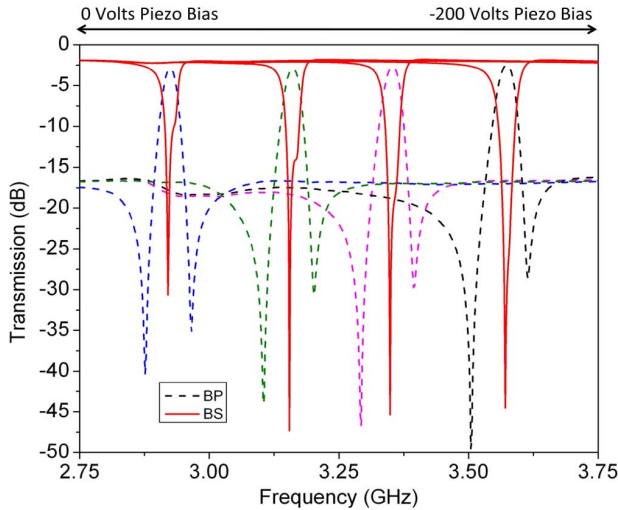


Fig. 12. Measured S_{21} response of the filter in bandpass and bandstop modes, tuned across the available tuning range.

to simulation, 0.1 dB of the loss was due to radiation from the coupling apertures. It can be seen that synthesis lines up well with measurement, noting that loss was not included in synthesis.

Group delay for each filter case can also be seen in Fig. 10. The filter in Fig. 10(a) has a 13.5-ns group delay in the middle of the passband, with 0.4-ns variation across the band. The filter in Fig. 10(b) has a 14.7-ns group delay in the middle of the passband, with 0.6-ns variation across the band. The self-equalized case has a greater group delay than the Butterworth case because it has a narrower bandwidth. The narrower bandwidth is a result of a reduction in M_{01} due to the use of an absorptive switch. For comparison, according to Agilent ADS, a Chebyshev filter with similar bandwidth as the self-equalized filter in Fig. 10(b) has a group delay of 18.2 ns in the middle of the passband.

Measured results showing a tunable elliptic bandpass S_{21} response and a tunable bandstop S_{21} response are shown in Fig. 12. Note that all traces in the plot are S_{21} . The responses in Fig. 12 were obtained using a solid-state reflective RF switch [18] in line with the transmission line between the resonators. While the loss is higher when using a solid-state switch, the filter can be switched between modes very quickly in this configuration, of the order of 10 ns. Comparatively, many MEMS switches have switching speeds on the order of 10 μ s. Fast switching speed between modes could be important in some situations, because the filter takes roughly 100 μ s to tune across the tuning range. For example, if a receiver was using the filter in bandpass mode at 3.5 GHz, and a signal appeared at 2.9 GHz that needed to be sensed quickly, the filter could switch to bandstop mode in 10 ns to make the receive path a through line at 2.9 GHz instead of taking 100 μ s to tune that bandpass filter to 2.9 GHz. This opens the receiver to a much wider frequency range, but, in some situations, the tradeoff would be justified.

In bandpass mode, the filter has less than 2.9 dB of insertion loss in the passband over the tuning range, which was 2.9–3.6 GHz. Up to 50 dB of isolation is demonstrated in the out-of-band transmission nulls, which are 1.5% away from the center of the passband. Beyond the transmission zeros,

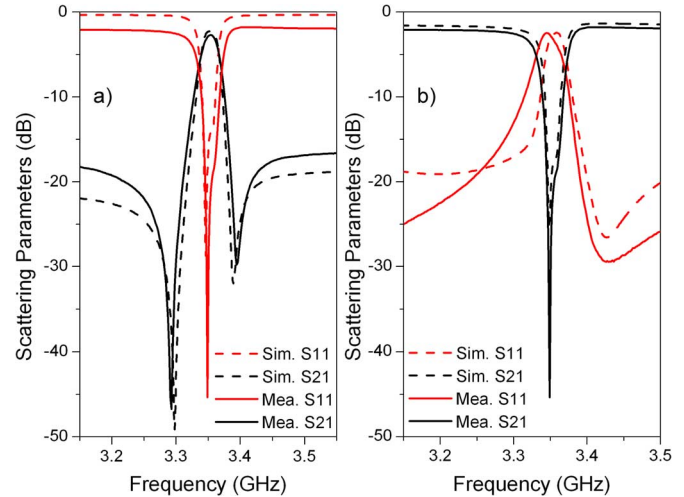


Fig. 13. Simulated versus measured data for the 3.35-GHz responses in Fig. 12. (a) Bandpass data. (b) Bandstop data.

the out-of-band attenuation was 17 dB. In bandstop mode, the filter produces up to 45 dB of isolation at its center frequency and has the same tuning range as in the bandpass case. Due to the higher resistance of the solid-state switch in its on state, the filter shows 1.8–2.4 dB of loss across the passband in the bandstop state.

Simulated versus measured data for the 3.35-GHz responses in Fig. 12 can be seen in Fig. 13. It can be seen that the simulated and measured responses are similar with only minor variation. The insertion loss and transmission zero locations relative to the passband in the bandpass mode were predicted very well. Similarly, the out-of-band loss in the bandstop mode of the filter lines up very well between measured and simulated data. However, there are a few discrepancies that warrant discussion. In the bandpass data, the measured S_{11} away from the passband is 1.7 dB lower than the simulated S_{11} . It is hypothesized that this is due to the finite off-state resistance of the switches on the source-to-load coupling transmission line. In the simulated bandpass data, the switches were modeled as 0.3-pF capacitors in the off-state as a first-order approximation according to the component datasheet. The finite resistance of the switches in their off-state causes the discrepancy in out-of-band isolation in the bandpass mode. In the bandstop mode, the switch was modeled as a 6- Ω resistor as a first-order approximation according to the component datasheet. The discrepancy in filter bandwidth can be attributed to the fact that the external coupling apertures were cut slightly too large by the circuit board plotter.

V. CONCLUSION

An electronically reconfigurable bandpass-to-bandstop filter was shown that can utilize the same set of coupled resonators and switch the feeding structure to change between different modes of operation. For example, the filter can exhibit Butterworth and elliptic bandpass responses as well as a Butterworth bandstop response by changing the state of the feed network and slightly adjusting the center frequencies of the resonators. The theory of such a filter was developed through the use of coupling matrices and coupling coefficients such that the inter-resonator

coupling remained unchanged. A detailed bandpass-to-bandstop filter design process was also presented. In bandpass mode, the fabricated filter had less than 3 dB of insertion loss for a 1.06% 3-dB bandwidth filter, and, in bandstop mode, the filter provided greater than 45 dB of isolation.

Benefits and applications of a bandpass-to-bandstop reconfigurable filter are envisioned to include general system flexibility at no cost of physical space, concurrent transmit and receive schemes, and multi-element antenna systems, but there are many other possible uses. In cognitive radio environments, these filters would be valuable to radio systems to isolate signals of interest or attenuate interfering signals, depending on the environment or mode of operation of the radio. This flexibility will be required since the electromagnetic environment of the future will be open and constantly changing.

ACKNOWLEDGMENT

The authors would like to thank H. H. Sigmarsson for providing fabrication expertise and guidance.

REFERENCES

- [1] B. Perlman, J. Laskar, and K. Lim, "Fine-tuning commercial and military radio design," *IEEE Microw. Mag.*, vol. 9, no. 4, pp. 95–106, Aug. 2008.
- [2] R. M. Young, J. D. Adam, C. R. Vale, T. T. Braggins, S. V. Krishnaswamy, C. E. Milton, D. W. Bever, L. G. Chorosinski, L.-S. Chen, D. E. Crockett, C. B. Freidhoff, S. H. Talisa, E. Capelle, R. Tranchini, J. R. Fende, J. M. Lorthioir, and A. R. Tories, "Low-loss bandpass RF filter using MEMS capacitance switches to achieve a one-octave tuning range and independently variable bandwidth," in *IEEE MTT-S Int. Microw. Symp. Dig.*, Philadelphia, PA, Jun. 2003, pp. 1781–1784.
- [3] H. Joshi, H. H. Sigmarsson, S. Moon, D. Peroulis, and W. J. Chappell, "High- Q fully reconfigurable tunable bandpass filters," *IEEE Trans. Microw. Theory Tech.*, vol. 57, no. 12, pp. 3525–3533, Dec. 2009.
- [4] D. R. Jachowski and C. Rauscher, "Frequency-agile bandstop filter with tunable attenuation," in *IEEE MTT-S Int. Microw. Symp. Dig.*, Boston, MA, Jun. 2009, pp. 649–652.
- [5] W.-H. Tu, "Switchable microstrip bandpass filters with reconfigurable on-state frequency responses," *IEEE Microw. Wireless Compon. Lett.*, vol. 20, no. 5, pp. 259–261, May 2010.
- [6] M. F. Karim, A. Q. Liu, A. Alphones, and A. B. Yu, "A novel reconfigurable filter using periodic structures," in *IEEE MTT-S Int. Microw. Symp. Dig.*, San Francisco, CA, Jun. 2006, pp. 943–946.
- [7] Y.-M. Chen, S.-F. Chang, C.-Y. Chou, and K.-H. Liu, "A reconfigurable bandpass-bandstop filter based on varactor-loaded closed-ring resonators [Technical Committee]," *IEEE Microw. Mag.*, vol. 10, no. 1, pp. 138–140, Feb. 2009.
- [8] H. C. Bell, "The coupling matrix in low-pass prototype filters," *IEEE Microw. Mag.*, vol. 8, no. 2, pp. 70–76, Apr. 2007.
- [9] J. Lee, E. J. Naglich, and W. J. Chappell, "Frequency response control in frequency-tunable bandstop filters," *IEEE Microw. Wireless Compon. Lett.*, accepted for publication.
- [10] S. Amari, "Direct synthesis of folded symmetric resonator filters with source-load coupling," *IEEE Microw. Wireless Compon. Lett.*, vol. 11, no. 6, pp. 264–266, Jun. 2001.
- [11] J. Lee and K. Sarabandi, "A miniaturized conductor-backed slot-line resonator filter with two transmission zeros," *IEEE Microw. Wireless Compon. Lett.*, vol. 16, no. 12, pp. 660–662, Dec. 2006.
- [12] H. Joshi, H. H. Sigmarsson, D. Peroulis, and W. J. Chappell, "Highly loaded evanescent cavities for widely tunable high- Q filters," in *IEEE MTT-S Int. Microw. Symp. Dig.*, Honolulu, HI, Jun. 2007, pp. 2133–2136.
- [13] J. S. Hong and M. J. Lancaster, *Microstrip Filters for RF/Microwave Applications*. New York: Wiley, 2001.
- [14] A. Khanna and Y. Garault, "Determination of loaded, unloaded, and external quality factors of a dielectric resonator coupled to a microstrip line," *IEEE Trans. Microw. Theory Tech.*, vol. MTT-31, no. 3, pp. 261–264, Mar. 1983.
- [15] R. S. Kwok and J.-F. Liang, "Characterization of high- Q resonators for microwave filter applications," *IEEE Trans. Microw. Theory Tech.*, vol. 47, no. 1, pp. 111–114, Jan. 1999.
- [16] J. B. Muldavin and G. M. Rebeiz, "Novel DC-contact MEMS shunt switches and high-isolation series/shunt designs," in *Proc. Eur. Microw. Conf.*, London, U.K., Sep. 2001, pp. 1–3.
- [17] "SPDT UltraCMOS RF switch 10–3000 MHz, absorptive," Peregrine Semiconductor. [Online]. Available: <http://www.peregrine-semi.com/pdf/datasheets/pe4251ds.pdf>.
- [18] "Surface mount microwave Schottky detector diodes," Avago Technol. [Online]. Available: <http://www.avagotech.com/docs/AV02-1388EN>



Eric J. Naglich (S'09) received the B.S. degree in electrical and computer engineering from Purdue University, West Lafayette, IN, in 2007, where he is currently working toward the Ph.D. degree in electrical and computer engineering under the direction of Prof. W. J. Chappell.

He was with GE Healthcare from 2007 to 2009, where he was involved with electromagnetic subsystem design in medical imaging and surgical navigation machines during the Edison Engineering Development Program. His current research focuses

on tunable filter synthesis and fabrication for widely tunable, adaptive RF front-ends in cognitive radio and radar applications.

Mr. Naglich is a member of the IEEE Microwave Theory and Techniques Society (IEEE MTT-S) and Eta Kappa Nu. He was the recipient of the 2nd Place Award in the 2010 IEEE MTT-S International Microwave Symposium Student Paper Competition.



Juseop Lee (A'02–M'03) received the B.E. and M.E. degrees in radio science and engineering from Korea University, Seoul, Korea, in 1997 and 1999, respectively, and the Ph.D. degree in electrical engineering from The University of Michigan, Ann Arbor, in 2009.

In 1999, he joined LG Information and Communications (now LG Electronics), Korea, where his activities included design and reliability analysis of RF components for code-division multiple-access (CDMA) cellular systems. In 2001, he joined the

Electronics and Telecommunications Research Institute (ETRI), Korea, where he was involved in designing passive microwave equipment for Ku - and Ka -band communications satellites. In 2005, he joined The University of Michigan, Ann Arbor, where he was as a Research Assistant and Graduate Student Instructor with the Radiation Laboratory, and his research activities focused on millimeter-wave radars and synthesis techniques for multiple-passband microwave filters. In 2009, he joined Purdue University, West Lafayette, IN, where he is currently a Post-Doctoral Research Associate, and his activities include the design of adaptable RF systems. His research interests include RF and microwave components, satellite transponders, and electromagnetic theories.

Dr. Lee was a recipient of the Highest Honor Award presented by Korea University, the Undergraduate Fellowship presented by Korea University, the Graduate Fellowship presented by LG Information and Communications, and the Graduate Fellowship presented by Korea Science and Engineering Foundation. He was a recipient of the Rackham Predoctoral Fellowship presented by the Rackham Graduate School, The University of Michigan. He was also the recipient of the IEEE Microwave Theory and Techniques Society (IEEE MTT-S) Graduate Fellowship. His coauthored paper received the 2nd place award in the 2010 IEEE MTT-S International Microwave Symposium Student Paper Competition. He is listed in *Who's Who in America*.



Dimitrios Peroulis (S'99–M'04) received the Ph.D. degree in electrical engineering from The University of Michigan, Ann Arbor, in 2003.

He has been with Purdue University, West Lafayette, IN, since August 2003, where he is currently leading a group of graduate students on a variety of research projects in the areas of RF microelectromechanical systems (MEMS), sensing, and power harvesting applications as well as RFID sensors for the health monitoring of sensitive equipment. He has been a Principal Investigator (PI) or a co-PI in numerous projects funded by government agencies and industry in these areas. He has authored or coauthored over 110 refereed journal and conference publications in the areas of microwave integrated circuits and antennas. He is currently a key contributor in two Defense Advanced Research Projects Agency (DARPA) projects at Purdue focusing on very high-quality ($Q > 1,000$) RF tunable filters in mobile form factors (DARPA Analog Spectral Processing Program, Phases I, II, and III) and on developing comprehensive characterization methods and models for understanding the viscoelasticity/creep phenomena in high-power RF MEMS devices (DARPA M/NEMS S&T Fundamentals Program, Phases I and II). Furthermore, he is leading the experimental program on the Center for the Prediction of Reliability, Integrity and Survivability of Microsystems (PRISM) funded by the National Nuclear Security Administration. In addition, he is heading the development of the MEMS technology in a U.S. Navy project (Marines) funded under the Technology Insertion Program for Savings (TIPS) program focused on harsh-environment wireless micro-sensors for the health monitoring of aircraft engines.

Dr. Peroulis was the recipient of the National Science Foundation CAREER Award in 2008. His students have received numerous student paper awards and other student research-based scholarships. He was also the recipient of eight teaching awards, including the 2010 HKN C. Holmes MacDonald Outstanding Teaching Award and the 2010 Charles B. Murphy award, which is Purdue University's highest undergraduate teaching honor.



William J. Chappell (S'98–M'02) received the B.S.E.E., M.S.E.E., and Ph.D. degrees from The University of Michigan, Ann Arbor, in 1998, 2000, and 2002, respectively.

He is currently an Associate Professor with the School of Electrical and Computer Engineering, Purdue University, West Lafayette, IN, where he is also a Member of the Birck Nanotechnology Center and the Center for Wireless Systems and Applications. His research focus is on advanced applications of RF and microwave components. He

has been involved with numerous Defense Advanced Research Projects Agency (DARPA) projects involved in advanced packaging and material processing for microwave applications. His research sponsors include HSARPA, the Office of Naval Research, the National Science Foundation, the state of Indiana, CERDEC, and ARO, as well as industry sponsors. His research group uses electromagnetic analysis, unique processing of materials, and advanced design to create novel microwave components. His specific research interests are the application of very high-quality and tunable components utilizing multilayer packages. In addition, he is involved with high-power RF systems, packages, and applications.

Dr. Chappell was the IEEE Microwave Theory and Techniques Society (IEEE MTT-S) Administrative Committee (AdCom) secretary for 2009 and was elected to the IEEE MTT-S AdCom for 2010–2012.

射频和天线设计培训课程推荐

易迪拓培训(www.edatop.com)由数名来自于研发第一线的资深工程师发起成立,致力并专注于微波、射频、天线设计研发人才的培养;我们于 2006 年整合合并微波 EDA 网(www.mweda.com),现已发展成为国内最大的微波射频和天线设计人才培养基地,成功推出多套微波射频以及天线设计经典培训课程和 ADS、HFSS 等专业软件使用培训课程,广受客户好评;并先后与人民邮电出版社、电子工业出版社合作出版了多本专业图书,帮助数万名工程师提升了专业技术能力。客户遍布中兴通讯、研通高频、埃威航电、国人通信等多家国内知名公司,以及台湾工业技术研究院、永业科技、全一电子等多家台湾地区企业。

易迪拓培训课程列表: <http://www.edatop.com/peixun/rfe/129.html>



射频工程师养成培训课程套装

该套装精选了射频专业基础培训课程、射频仿真设计培训课程和射频电路测量培训课程三个类别共 30 门视频培训课程和 3 本图书教材;旨在引领学员全面学习一个射频工程师需要熟悉、理解和掌握的专业知识和研发设计能力。通过套装的学习,能够让学员完全达到和胜任一个合格的射频工程师的要求...

课程网址: <http://www.edatop.com/peixun/rfe/110.html>

ADS 学习培训课程套装

该套装是迄今国内最全面、最权威的 ADS 培训教程,共包含 10 门 ADS 学习培训课程。课程是由具有多年 ADS 使用经验的微波射频与通信系统设计领域资深专家讲解,并多结合设计实例,由浅入深、详细而又全面地讲解了 ADS 在微波射频电路设计、通信系统设计和电磁仿真设计方面的内容。能让您在最短的时间内学会使用 ADS,迅速提升个人技术能力,把 ADS 真正应用到实际研发工作中去,成为 ADS 设计专家...



课程网址: <http://www.edatop.com/peixun/ads/13.html>



HFSS 学习培训课程套装

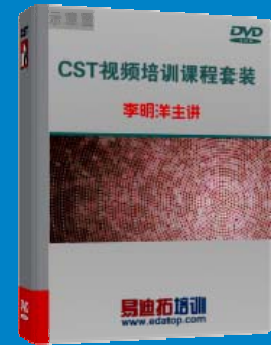
该套课程套装包含了本站全部 HFSS 培训课程,是迄今国内最全面、最专业的 HFSS 培训教程套装,可以帮助您从零开始,全面深入学习 HFSS 的各项功能和在多个方面的工程应用。购买套装,更可超值赠送 3 个月免费学习答疑,随时解答您学习过程中遇到的棘手问题,让您的 HFSS 学习更加轻松顺畅...

课程网址: <http://www.edatop.com/peixun/hfss/11.html>

CST 学习培训课程套装

该培训套装由易迪拓培训联合微波 EDA 网共同推出,是最全面、系统、专业的 CST 微波工作室培训课程套装,所有课程都由经验丰富的专家授课,视频教学,可以帮助您从零开始,全面系统地学习 CST 微波工作的各项功能及其在微波射频、天线设计等领域的设计应用。且购买该套装,还可超值赠送 3 个月免费学习答疑...

课程网址: <http://www.edatop.com/peixun/cst/24.html>



HFSS 天线设计培训课程套装

套装包含 6 门视频课程和 1 本图书,课程从基础讲起,内容由浅入深,理论介绍和实际操作讲解相结合,全面系统的讲解了 HFSS 天线设计的全过程。是国内最全面、最专业的 HFSS 天线设计课程,可以帮助您快速学习掌握如何使用 HFSS 设计天线,让天线设计不再难...

课程网址: <http://www.edatop.com/peixun/hfss/122.html>

13.56MHz NFC/RFID 线圈天线设计培训课程套装

套装包含 4 门视频培训课程,培训将 13.56MHz 线圈天线设计原理和仿真设计实践相结合,全面系统地讲解了 13.56MHz 线圈天线的工作原理、设计方法、设计考量以及使用 HFSS 和 CST 仿真分析线圈天线的具体操作,同时还介绍了 13.56MHz 线圈天线匹配电路的设计和调试。通过该套课程的学习,可以帮助您快速学习掌握 13.56MHz 线圈天线及其匹配电路的原理、设计和调试...

详情浏览: <http://www.edatop.com/peixun/antenna/116.html>



我们的课程优势:

- ※ 成立于 2004 年,10 多年丰富的行业经验,
- ※ 一直致力并专注于微波射频和天线设计工程师的培养,更了解该行业对人才的要求
- ※ 经验丰富的一线资深工程师讲授,结合实际工程案例,直观、实用、易学

联系我们:

- ※ 易迪拓培训官网: <http://www.edatop.com>
- ※ 微波 EDA 网: <http://www.mweda.com>
- ※ 官方淘宝店: <http://shop36920890.taobao.com>